Supplemental Document

Optics EXPRESS

Subsampling strategies for compressive Hadamard single-pixel imaging: supplement

C. THOMAS,[1,*] N. DUCROS,[2,3] J. E. COHEN,[2] L. JACQUES,[4,5] AND M. GEORGES[1]

[1]*Centre Spatial de Liège, STAR Institute, Université de Liège, Liège, Belgium*
[2]*INSA-Lyon, Université Claude Bernard Lyon 1, CNRS, Inserm, CREATIS UMR 5220, UI294, F-69691, Lyon, France*
[3]*Institut Universitaire de France (IUF), France*
[4]*INMA/ICTEAM, UCLouvain, Louvain-la-Neuve, Belgium*
[5]*INRIA chair at Collegium de Lyon, OCKHAM, ENS, France*
[*]*clement.thomas@uliege.be*

This supplement published with Optica Publishing Group on 2 October 2026 by The Authors under the terms of the Creative Commons Attribution 4.0 License in the format provided by the authors and unedited. Further distribution of this work must maintain attribution to the author(s) and the published article's title, journal citation, and DOI.

Supplement DOI: https://doi.org/10.6084/m9.figshare.33592087

Parent Article DOI: https://doi.org/10.1364/OE.608747

Subsampling strategies for compressive Hadamard single-pixel imaging: supplemental document

1. NOISE MODEL

We want the noise model to be consistent with a realistic SPI setup that employs a DMD. In practice, such systems present essentially a Poisson shot noise $n_P \sim \mathcal{P}(\boldsymbol{H}_\Omega \boldsymbol{x})$, and an additional Gaussian read noise $n_G \sim \mathcal{N}(0, \sigma_r^2)$. Practically, the Hadamard projections are obtained by first applying the positive part of the patterns ($\boldsymbol{H}_\Omega^+ = (\boldsymbol{H}_\Omega + 1)/2$) on the DMD, then the negative parts ($\boldsymbol{H}_\Omega^- = |(\boldsymbol{H}_\Omega - 1)/2|$), and finally subtracting the negative measurements from the positive ones. Positive measurements can be written as

$$\boldsymbol{y}^+ = \mathcal{P}(\boldsymbol{H}_\Omega^+ \boldsymbol{x}) + \mathcal{N}(0, \sigma_r^2), \tag{S1}$$

and a thresholding operator is applied to the right-hand side of (S1) to avoid negative values. The amount of photons in one measurement $\lambda_i^+ = \langle \boldsymbol{H}_i^+, \boldsymbol{x} \rangle$ is, in principle, pattern-dependent. However, since each row of $\boldsymbol{H}_\Omega^+$ contains exactly N/2 non-zero entries (except for the first pattern), the expected photon count per measurement satisfies $\lambda_i^+ \approx \sum_{n=1}^{N} (\boldsymbol{x}_n)/2$, which is approximately constant across measurements. This justifies approximation of the Poisson shot noise as $\mathcal{P}(\boldsymbol{H}_\Omega^+ \boldsymbol{x}) \approx \boldsymbol{H}_\Omega^+ \boldsymbol{x} + \mathcal{P}(\lambda^+)$. In the high-flux approximation, this is equivalent to an additive Gaussian noise such that $\mathcal{P}(\boldsymbol{H}_\Omega^+ \boldsymbol{x}) = \boldsymbol{H}_\Omega^+ \boldsymbol{x} + \mathcal{N}(0, \lambda^+)$. The same reasoning is applied to the negative measurements, and considering the structure of the Hadamard patterns and the high-flux approximation, we have $\lambda = \lambda^+ \approx \lambda^-$. Thus, positive and negative measurement vectors can be written

$$\begin{aligned} \boldsymbol{y}^+ &= \boldsymbol{H}_\Omega^+ \boldsymbol{x} + \mathcal{N}(0, \lambda + \sigma_r^2), \\ \boldsymbol{y}^- &= \boldsymbol{H}_\Omega^- \boldsymbol{x} + \mathcal{N}(0, \lambda + \sigma_r^2), \end{aligned} \tag{S2}$$

and a thresholding operator is applied to avoid negative entries in both measurement vectors. Finally, positive and negative values are subtracted in post-processing such that

$$\boldsymbol{y} = \boldsymbol{y}^+ - \boldsymbol{y}^- = \boldsymbol{H}_\Omega \boldsymbol{x} + \mathcal{N}\big(0, 2(\lambda + \sigma_r^2)\big). \tag{S3}$$

Hence, the homogeneity of the Poisson contribution, combined with this high-flux approximation, justifies treating the effective measurement errors $\boldsymbol{e}$ as additive Gaussian noise with fixed variance $\sigma^2 = 2(\lambda + \sigma_r^2)$. This noise model is a valid approximation only when $\lambda \gg \sigma_r$, which is a reasonable assumption in the high-flux approximation.

We will test the strategies with several noise levels. For physical interpretability, it is interesting to work at a fixed measurement signal-to-noise ratio (SNR) rather than arbitrarily fix the variance σ^2. First, we define the SNR as

$$10\log_{10}\left(\frac{\|\boldsymbol{y}_{\text{clean}}\|_2^2}{\mathbb{E}\|\boldsymbol{e}\|_2^2}\right), \tag{S4}$$

where $\|\boldsymbol{y}_{\text{clean}}\|_2^2$ is the signal power, and $\mathbb{E}\|\boldsymbol{e}\|_2^2$ is the noise power. Since $\boldsymbol{e} \sim \mathcal{N}(0, \sigma^2)$, then $\mathbb{E}\|\boldsymbol{e}\|_2^2 = \sum_{i=1}^{M} \mathbb{E}[e_i^2] = M\sigma^2$, and we can determine σ at fixed SNR with

$$\sigma^2 = \frac{\|\boldsymbol{y}_{\text{clean}}\|_2^2}{M 10^{\text{SNR}/10}}. \tag{S5}$$

2. RESULTS

Table S1. Mean ranking and standard deviations of each strategy at 10%, 25%, and 50% SR, with pseudoinverse reconstruction, and without measurement noise. For each image, the PSNR values of all strategies are ranked from 1 (best) to 15 (worst), and the mean rank of each strategy is computed over the entire dataset. The mean PSNR in dB is added between parentheses as an indicator.

Scheme	Order	10%	25%	50%
Spread Spectrum		$15.0 \pm 0.0(12.1)$	$14.9 \pm 1.2(13.0)$	$14.8 \pm 0.8(14.7)$
Scrambled		$14.4 \pm 1.2(13.5)$	$14.6 \pm 1.2(13.7)$	$14.9 \pm 1.0(14.1)$
DET	Seq	$2.2 \pm 0.8(22.3)$	$2.8 \pm 0.7(25.3)$	$2.7 \pm 0.6(30.4)$
	TV	$3.2 \pm 0.9(22.2)$	$3.5 \pm 1.0(25.3)$	$4.0 \pm 0.5(29.4)$
	CC	$3.4 \pm 1.1(22.1)$	$2.5 \pm 1.0(25.7)$	$1.8 \pm 0.9(30.6)$
	Var	$\mathbf{1.4} \pm 0.7(22.5)$	$\mathbf{1.3} \pm 0.6(25.9)$	$\mathbf{1.6} \pm 0.5(30.6)$
VDS	Unif	$14.2 \pm 0.5(13.8)$	$14.0 \pm 0.7(14.6)$	$13.2 \pm 0.4(18.1)$
	Seq	$11.0 \pm 0.1(18.1)$	$11.0 \pm 0.0(20.6)$	$11.0 \pm 0.0(24.6)$
	TV	$12.0 \pm 0.1(18.0)$	$12.0 \pm 0.0(20.3)$	$12.0 \pm 0.0(24.1)$
	CC	$9.9 \pm 0.4(19.9)$	$9.2 \pm 0.9(23.3)$	$5.3 \pm 0.8(27.9)$
	Var	$8.9 \pm 0.5(20.5)$	$9.5 \pm 0.6(23.3)$	$7.7 \pm 1.1(27.5)$
MDS	Seq	$6.1 \pm 0.8(21.4)$	$7.0 \pm 1.2(24.0)$	$8.5 \pm 1.2(27.1)$
	TV	$6.6 \pm 1.0(21.3)$	$6.7 \pm 1.2(24.1)$	$9.0 \pm 1.3(27.0)$
	CC	$7.8 \pm 1.1(20.9)$	$7.0 \pm 1.2(24.0)$	$8.0 \pm 1.5(27.4)$
	Var	$5.5 \pm 0.9(21.6)$	$5.5 \pm 0.8(24.4)$	$6.4 \pm 1.0(27.7)$

Table S2. Mean ranking and standard deviations of each strategy at 10%, 25%, and 50% SR, with ISTA reconstruction, and without measurement noise. For each image, the PSNR values of all strategies are ranked from 1 (best) to 15 (worst), and the mean rank of each strategy is computed over the entire dataset. The mean PSNR in dB is added between parentheses as an indicator.

Scheme	Order	10%	25%	50%
Spread Spectrum		$13.3 \pm 1.0(18.0)$	$13.0 \pm 1.0(21.2)$	$13.3 \pm 0.7(26.1)$
Scrambled		$12.8 \pm 0.9(18.2)$	$13.1 \pm 1.0(21.2)$	$13.2 \pm 0.8(26.1)$
DET	Seq	$\mathbf{1.7} \pm 0.8(23.5)$	$2.2 \pm 1.2(26.7)$	$2.0 \pm 1.1(31.6)$
	TV	$2.3 \pm 1.0(23.5)$	$2.9 \pm 1.5(26.6)$	$3.7 \pm 1.4(31.2)$
	CC	$4.8 \pm 1.5(22.7)$	$3.9 \pm 1.6(26.4)$	$3.2 \pm 1.4(31.4)$
	Var	$2.3 \pm 0.9(23.4)$	$\mathbf{2.0} \pm 1.0(26.8)$	$\mathbf{1.8} \pm 1.1(31.6)$
VDS	Unif	$15.0 \pm 0.0(14.0)$	$15.0 \pm 0.0(16.0)$	$15.0 \pm 0.0(21.2)$
	Seq	$11.4 \pm 0.7(18.8)$	$11.4 \pm 0.7(21.9)$	$11.1 \pm 0.6(27.3)$
	TV	$12.5 \pm 0.8(18.7)$	$12.5 \pm 0.8(21.7)$	$12.3 \pm 0.8(26.8)$
	CC	$9.9 \pm 0.5(20.9)$	$9.5 \pm 0.9(24.7)$	$6.0 \pm 1.6(30.0)$
	Var	$8.7 \pm 0.6(21.5)$	$9.3 \pm 0.6(24.7)$	$7.4 \pm 1.7(29.7)$
MDS	Seq	$5.3 \pm 1.1(22.6)$	$5.7 \pm 1.3(25.9)$	$7.1 \pm 1.8(29.7)$
	TV	$5.9 \pm 1.3(22.5)$	$6.0 \pm 1.4(25.8)$	$7.5 \pm 1.9(29.6)$
	CC	$8.1 \pm 1.0(21.7)$	$7.6 \pm 1.2(25.4)$	$9.2 \pm 1.3(29.4)$
	Var	$6.0 \pm 1.0(22.5)$	$6.0 \pm 1.2(25.9)$	$7.0 \pm 1.4(29.8)$

Table S3. Mean ranking and standard deviations of each strategy at 10%, 25%, and 50% SR, with PinvNet reconstruction, and without measurement noise. For each image, the PSNR values of all strategies are ranked from 1 (best) to 15 (worst), and the mean rank of each strategy is computed over the entire dataset. The mean PSNR in dB is added between parentheses as an indicator.

Scheme	Order	10%	25%	50%
Spread Spectrum		$13.0 \pm 0.2 (16.8)$	$13.0 \pm 0.2 (18.4)$	$13.2 \pm 0.4 (20.3)$
Scrambled		$14.4 \pm 0.5 (14.0)$	$14.7 \pm 0.5 (14.8)$	$15.0 \pm 0.2 (16.6)$
DET	Seq	$\mathbf{1.7} \pm 0.7 (23.8)$	$\mathbf{1.4} \pm 0.6 (27.0)$	$\mathbf{1.3} \pm 0.5 (30.2)$
	TV	$2.0 \pm 0.9 (23.7)$	$2.1 \pm 0.8 (26.9)$	$2.3 \pm 1.0 (30.1)$
	CC	$5.2 \pm 1.2 (22.8)$	$3.8 \pm 0.8 (26.3)$	$3.1 \pm 0.9 (30.0)$
	Var	$2.4 \pm 0.9 (23.6)$	$2.8 \pm 0.6 (26.7)$	$3.3 \pm 0.7 (30.0)$
VDS	Unif	$14.6 \pm 0.5 (14.0)$	$14.3 \pm 0.5 (15.1)$	$13.9 \pm 0.4 (19.0)$
	Seq	$11.1 \pm 0.3 (18.8)$	$11.1 \pm 0.3 (21.6)$	$11.0 \pm 0.0 (25.7)$
	TV	$11.9 \pm 0.3 (18.7)$	$11.9 \pm 0.3 (21.4)$	$12.0 \pm 0.0 (25.1)$
	CC	$9.9 \pm 0.2 (20.6)$	$9.6 \pm 0.6 (24.2)$	$6.8 \pm 1.4 (28.3)$
	Var	$8.9 \pm 0.5 (21.2)$	$9.3 \pm 0.5 (24.3)$	$8.6 \pm 1.1 (28.1)$
MDS	Seq	$5.0 \pm 0.9 (22.8)$	$5.8 \pm 0.9 (25.6)$	$6.5 \pm 1.3 (28.4)$
	TV	$5.2 \pm 1.1 (22.8)$	$5.8 \pm 0.9 (25.6)$	$6.2 \pm 1.5 (28.4)$
	CC	$8.1 \pm 0.6 (21.5)$	$7.8 \pm 0.7 (24.9)$	$9.1 \pm 1.3 (28.0)$
	Var	$6.6 \pm 0.8 (22.5)$	$6.6 \pm 0.8 (25.4)$	$7.8 \pm 1.1 (28.2)$

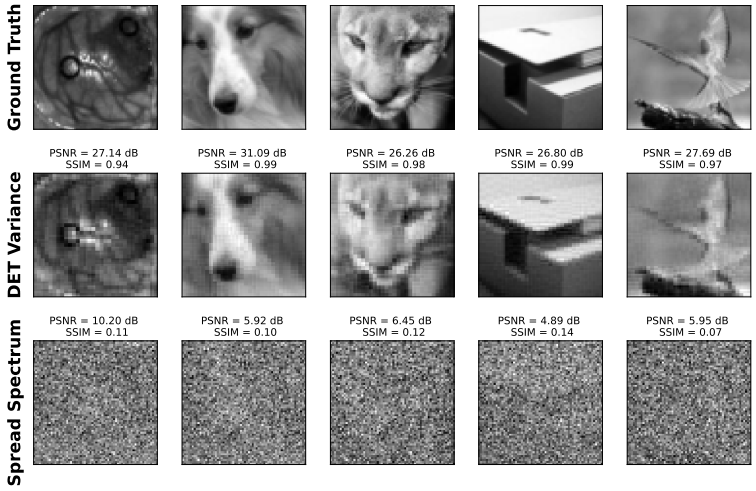

Fig. S1. Pseudoinverse reconstructions at 25% SR from noiseless measurements for the best (deterministic scheme with the variance ordering) and worst (spread spectrum) strategies.

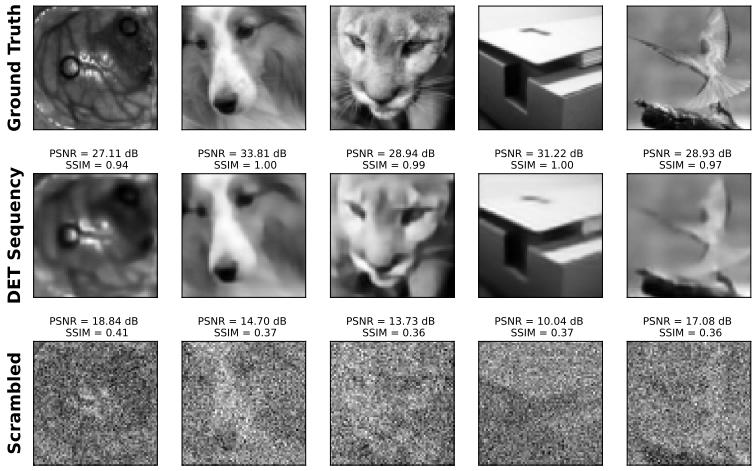

Fig. S2. PinvNet reconstructions at 25% SR from noiseless measurements for the best (deterministic scheme with the sequency ordering) and worst (scrambled Hadamard) strategies.

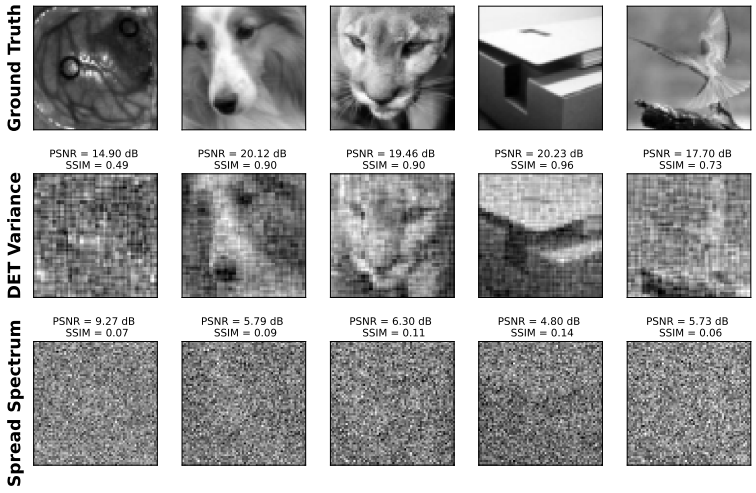

Fig. S3. Pseudoinverse reconstructions at 25% SR and with added Gaussian noise corresponding to a 15 dB measurement SNR for the best (deterministic scheme with the variance ordering) and worst (spread spectrum) strategies.

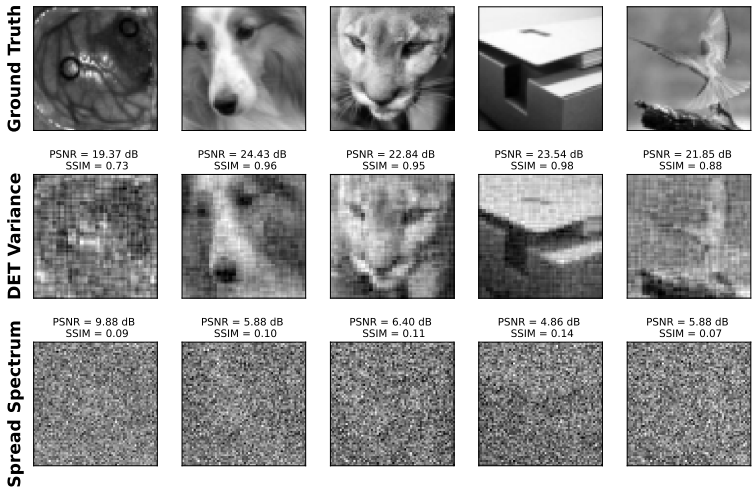

Fig. S4. Pseudoinverse reconstructions at 25% SR and with added Gaussian noise corresponding to a 20 dB measurement SNR for the best (deterministic scheme with the variance ordering) and worst (spread spectrum) strategies.

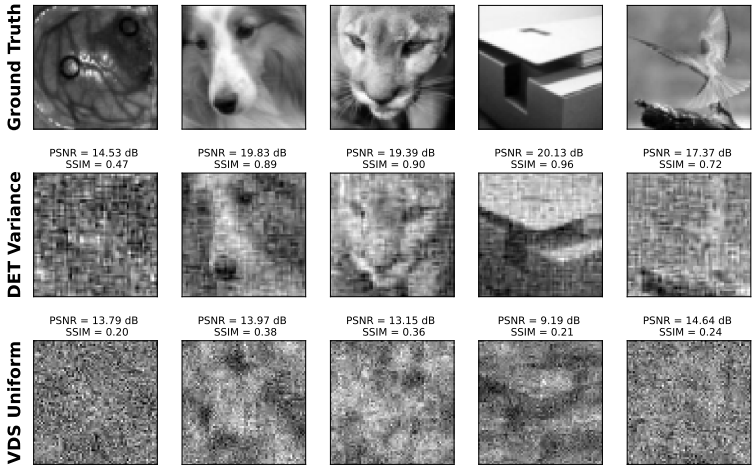

Fig. S5. ISTA reconstructions at 25% SR and with added Gaussian noise corresponding to a 15 dB measurement SNR for the best (deterministic scheme with the variance ordering) and worst (uniform sampling) strategies.

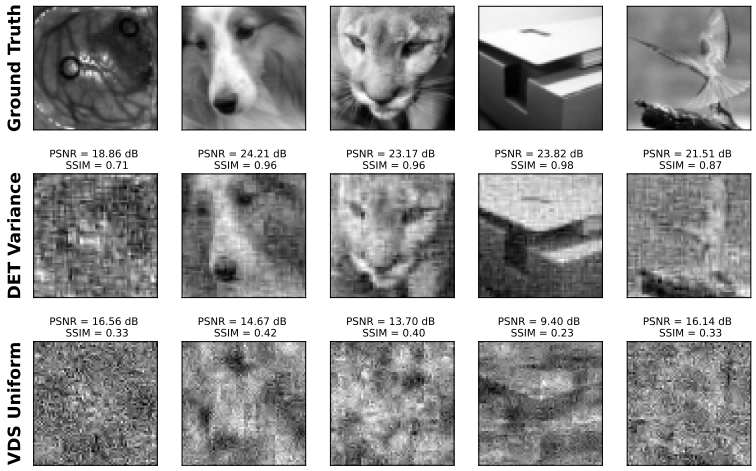

Fig. S6. ISTA reconstructions at 25% SR and with added Gaussian noise corresponding to a 20 dB measurement SNR for the best (deterministic scheme with the variance ordering) and worst (uniform sampling) strategies.

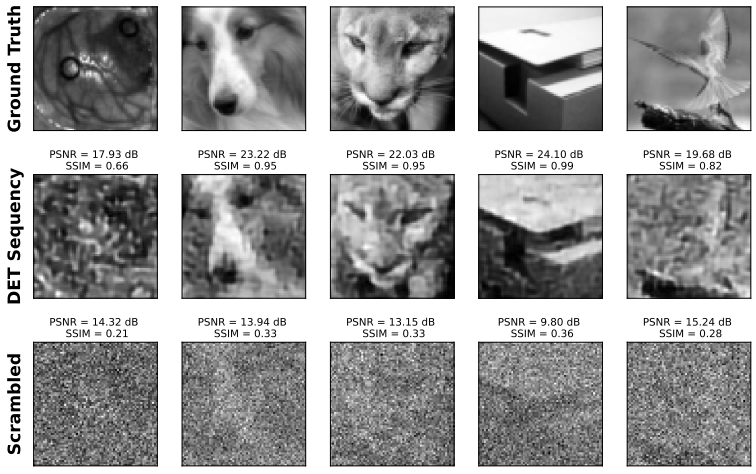

Fig. S7. PinvNet reconstructions at 25% SR and with added Gaussian noise corresponding to a 15 dB measurement SNR for the best (deterministic scheme with the sequency ordering) and worst (scrambled Hadamard) strategies.

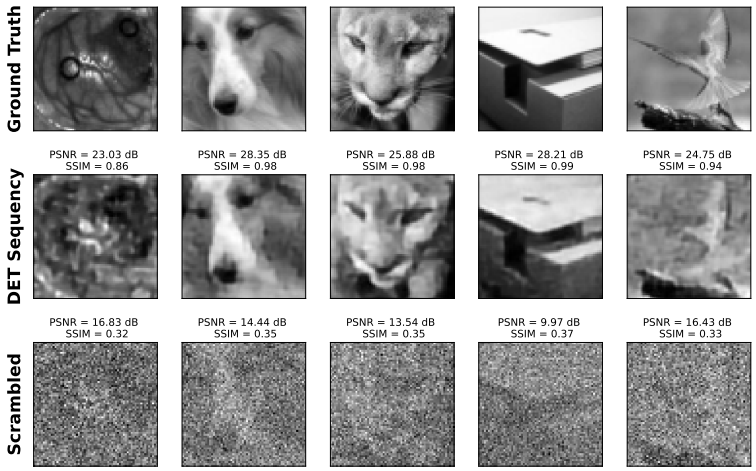

Fig. S8. PinvNet reconstructions at 25% SR and with added Gaussian noise corresponding to a 20 dB measurement SNR for the best (deterministic scheme with the sequency ordering) and worst (scrambled Hadamard) strategies.

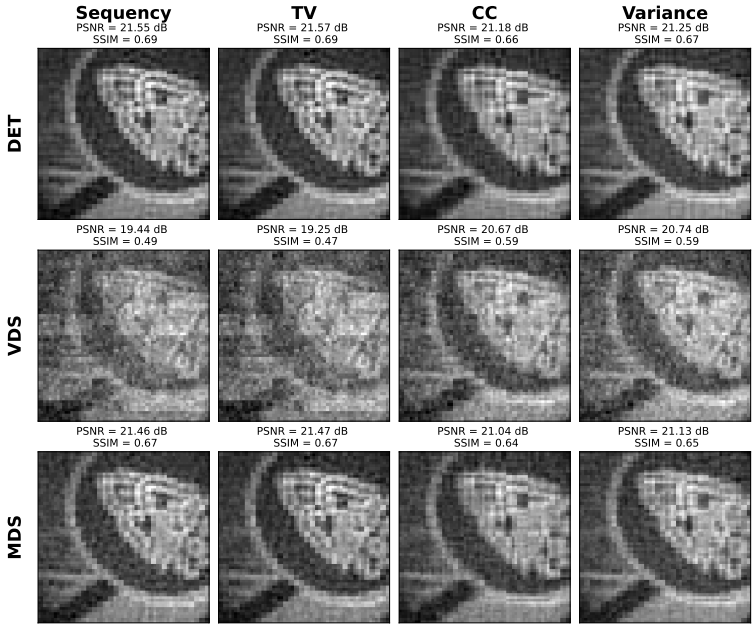

Fig. S9. Pseudoinverse reconstructions from experimental data at 25% SR, with 20 integrated channels from 552.53 nm to 554.96 nm. They are presented in matrix form with the subsampling scheme on the vertical axis and the associated metric on the horizontal axis.

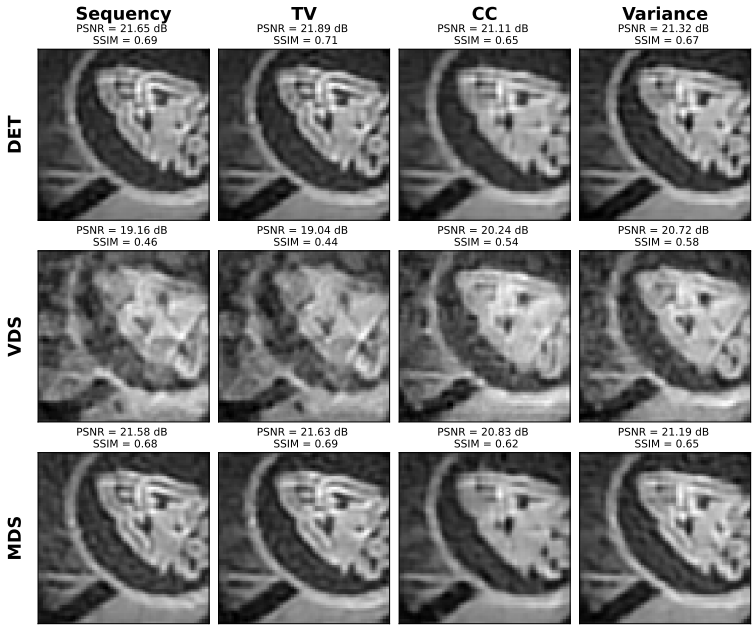

Fig. S10. PinvNet reconstructions from experimental data at 25% SR, with 20 integrated channels from 552.53 nm to 554.96 nm. They are presented in matrix form with the subsampling scheme on the vertical axis and the associated metric on the horizontal axis.